Deducing Rock Properties from Spectral Seismic Data - Final Report

Jiajun Han, Maria-Veronica Ciocanel, Heather Hardeman, Dillon Nasserden, Byungjae Son, and Shuai Ye

Abstract Seismic data collection and analysis is essential in the identification of hydrocarbon resources in the subsurface of the earth. Non-stationary seismic signals obtained from a series of seismic sources are often analyzed using standard as well as spectral decomposition attributes that can help determine the location of various reservoirs and channels. We compare the performance of standard attributes such as derivatives of the envelope trace with time-frequency attributes such as amplitude and phase. We conclude that the basis pursuit method with Ricker wavelets provides the best localization results for spectral decomposition of examples of post-stack reservoir and valley data. For pre-stack data, we initially consider traditional constant-frequency amplitude versus offset (AVO) attributes. In reality, amplitude is often dependent on frequency so that the analysis of seismic data may require the use

Jiajun Han
Hampson-Russell, Geosoftware, CGG, Calgary, AB, Canada, e-mail: Jiajun.Han@cgg.com

Maria-Veronica Ciocanel
Division of Applied Mathematics, Brown University, Providence, RI, USA, e-mail: veronica_ciocanel@brown.edu

Heather Hardeman
Department of Mathematics and Statistics, University of Calgary, Calgary, AB, Canada, e-mail: heather.hardeman@ucalgary.ca

Dillon Nasserden
Department of Mathematics and Statistics, Simon Fraser University, Vancouver, BC, Canada, e-mail: dnasserd@sfu.ca

Byungjae Son
Department of Mathematics and Statistics, University of North Carolina at Greensboro, Greensboro, NC, USA, e-mail: b_son@uncg.edu

Shuai Ye
Department of Mathematics, Texas A & M University, College Station, TX, USA, e-mail: yes1989@math.tamu.edu

of frequency-dependent AVO techniques. We propose two such methods that extend different approximation equations of the seismic reflected waves in terms of angles of incidence and use basis pursuit for spectral decomposition. Attributes given by these methods are able to identify the location of the reservoir in the pre-stack data considered and have the advantage of better resolution while varying frequency.

1 Introduction

The propagation of a seismic wave through a complex medium causes the frequency content of seismic signals to vary in time, resulting in a non-stationary frequency character for the recorded data. Spectral decomposition, also called time-frequency decomposition, aims to characterize the change in frequency with time of a seismic signal traveling through the earth's subsurface. This procedure of time-frequency mapping is non-unique as there exists various methods to analyze the time-frequency content of non-stationary signals. Here, we are concerned with the time-frequency analysis of four methods, namely, the short time Fourier transform $(STFT)$, the continuous wavelet transform (CWT), the synchrosqueezing transform (SST) and the method of basis pursuit (BP). The seismic data examined included both post-stack and pre-stack data. The aim of our investigations is to find evidence for subsurface reservoirs and other geological structures for both classes of data using a combination of the four time-frequency methods and several seismic attributes.

The mathematical preliminaries concerning the foundation of the four transform methods are described in section 2, beginning with the most standard method $(STFT)$ and ending with the most exotic (BP). Subsequently, we will introduce a class of seismic attributes under the general category of complex trace analysis. An overview of geological data acquisition methods and procedures is then outlined in section 3, beginning with simple ray-based concepts and ending with the procedures of geological data stacking. Numerical examination of the data follows for both pre-stack and post-stack data samples in sections 4 and 5. We then move to amplitude versus offset (AVO) analysis to analyze pre-stack seismic data. Lastly, we conclude with a discussion of future research.

2 Spectral decomposition methods and trace analysis attributes

2.1 Short time Fourier transform

The Fourier transform (FT) of a signal, $s(t)$, is defined to be

$$F_s(f) = \int_{-\infty}^{\infty} s(t) e^{-2i\pi ft} \mathrm{d}t \tag{1}$$

where t is time, f is frequency and $i = \sqrt{-1}$. While the Fourier transform contains all the information to reconstruct any signal, in many applications one can only see the amplitude spectrum, which hides the time location of any particular frequency component. Thus the Fourier transform performs poorly on signals that are not stationary. This is the motivation for the development of the $STFT$. In the $STFT$, we multiply the signal by a window function which is nonzero only for a short period of time. The signal is transformed as the window is translated across the time-axis. If the window is sufficiently narrow, each part of $s(t)$ can be viewed as stationary so that the Fourier transform can be used, allowing us to extract local time-frequency information. Mathematically, the $STFT$ of the signal can be expressed as

$$S_s(f,\tau) = \int_{-\infty}^{\infty} s(t)w(t-\tau)e^{-2i\pi ft}\mathrm{d}t, \tag{2}$$

corresponding to the Fourier transform of $s(t)$, tapered by the window function, $w(t)$, see Cohen (1995) [8]. The parameter τ is the delay time to the center of the taper, or equivalently, to the center of the interval to be transformed.

2.2 Continuous wavelet transform

Continuous wavelet transform (CWT) is another method used to analyze the time-frequency content of a signal. Unlike the $STFT$ where the window function has a fixed length, the CWT uses a variable window length. If the length of the interval on which the window function is nonzero increases, the time resolution decreases and the frequency resolution increases. Alternatively, when the length of the interval decreases, the time resolution increases and the frequency resolution decreases. Essentially, the variable length of the window function allows for a better trade off between time-frequency localization of the signal, see Sinha (2002) [14].

The building blocks of the wavelet transform are wavelets which are functions, $\psi(t) \in L^2(\mathbb{R})$, that have zero mean and are localized in both time and frequency, i.e., no matter how small we take the support of the window function, all the frequencies of an individual wavelet will be contained in the interval. This is similar to the $STFT$, in that, it also is localized in time and frequency, but there are issues with the time-frequency resolution trade-off.

Each wavelet basis is generated by dilating and translating a two parameter function known as the mother wavelet, $\psi(t)$. Given a wavelet basis, we can represent all functions in the basis by translations and scalings of the mother wavelet

$$\left\{ \frac{1}{\sqrt{a}}\psi\left(\frac{t-\tau}{a}\right) \right\} \tag{3}$$

where $a, \tau \in \mathbb{R}$ and $a \neq 0$. The parameter a is called the dilation parameter or scale and τ is called the translation parameter which are related to the frequency and time location, respectively. The wavelet transform of a signal, $s(t)$, takes the form

$$W_s(a,\tau) = \frac{1}{\sqrt{a}} \int_{-\infty}^{\infty} s(t)\psi^* \left(\frac{t-\tau}{a} \right) \mathrm{d}t\,, \tag{4}$$

where ψ^* is the complex conjugate of the mother wavelet, Daubechies (1992) [9].

2.3 Synchrosqueezing transform

Synchrosqueezing transform (SST) combines the CWT and the instantaneous frequencies with a reassignment step to concentrate the energy around the ridges in the time-frequency representation of the signal, see Auger et al. (1995) [2]. We assume that the signal, $s(t)$, is the sum of individual time-varying harmonic components, i.e.,

$$s(t) = \sum_{k=1}^{N} A_k(t)\cos[\theta_k(t)] + \eta(t) \tag{5}$$

where, $A_k(t)$, is the instantaneous amplitude and N is the maximum number of components making up the signal. The instantaneous frequency, $f_k(t)$, of the signal component k, is defined to be

$$f_k(t) = \frac{1}{2\pi}\frac{\mathrm{d}}{\mathrm{d}t}\theta_k(t). \tag{6}$$

We would like to concentrate the time-frequency map into the most representative instantaneous frequencies which may decrease spectral smearing of the signal while also allowing for signal reconstruction. In CWT, the variable length of the window, on which the mother wavelet is nonzero results in greater signal resolution but does not prevent spectral smearing in the time-frequency plane. By focusing the time-frequency coefficients into instantaneous frequencies, SST improves the resolution of the signal. We define the derivative of the wavelet transform at the point, (a,τ), with respect to τ for all, $W_s(a,\tau) \neq 0$, as

$$w_s(a,\tau) = \frac{-i}{2\pi W_s(a,\tau)}\frac{\partial}{\partial \tau} W_s(a,\tau). \tag{7}$$

Note that the ridges in the time-frequency domain represent the instantaneous frequencies of (7). The aim now is to squeeze the frequencies around these ridges in order to reduce spectral smearing. We accomplish this by the following map

$$(a,\tau) \to (w_s(a,\tau),\tau) \tag{8}$$

where the above mapping is called synchrosqueezing. The SST coefficient $T_s(w,\tau)$ is determined only at the centers, w_j, of the frequency range $[w_j - \Delta w/2, w_j + \Delta w/2]$, where $\Delta w = w_j - w_{j-1}$ and

$$T_s(w_j,\tau) = \frac{1}{\Delta w}\sum_{a_k} W_s(a_k,\tau)a^{-3/2}\Delta a_k, \tag{9}$$

where a_k must satisfy $|w(a_k,\tau) - w_j| \leq \Delta w/2$, see Wu et al. (2011) [20], Li et al. (2012) [11].

2.4 Basis pursuit

The main principle of BP is to decompose a signal into individual atoms from a predefined dictionary. It includes a minimization term to reduce the number and magnitudes of retrieved atoms, yielding a sparse representation, see Chen et al. (2001) [7]. Also, it identifies all atoms simultaneously by casting both steps into a single inversion problem, see Bonar et al. (2010) [3], Zhang et al. (2011) [22], Vera Rodriguez et al. (2012) [17]. The signal, $s(t)$, is represented as the convolution of a family of wavelets $\psi(t,n)$ and its associated coefficient series $a(t,n)$ as

$$s(t) = \sum_{n=1}^{N} [\psi(t,n) * a(t,n)] \tag{10}$$

where N is the number of atoms, t is time, and n is the dilation of atom $\psi(t,n)$ determining its frequency. Using matrix notation, equation (10) can be rewritten as

$$\mathbf{s} = \begin{pmatrix} \Psi_1 & \Psi_2 & \dots & \Psi_N \end{pmatrix} \begin{pmatrix} a_1 \\ a_2 \\ \vdots \\ a_N \end{pmatrix} + \eta = D\mathbf{a} + \eta \tag{11}$$

where Ψ_n denotes the convolution matrix of $\psi(t,n)$ with dilation index n, D is the wavelet dictionary, and η is the noise. The time-frequency distribution of BP corresponds to the set of weights $\mathbf{a}$ associated with the set of atoms $\psi(t,n)$ coming from the dictionary D.

We define the cost function

$$J = \frac{1}{2}\|\mathbf{s} - D\mathbf{a}\|_2^2 + \lambda\|\mathbf{a}\|_1. \tag{12}$$

The first term of J represents the data misfit term based on the l_2 norm, that is, the least-squares difference between the observed and predicted data, whereas the second term of J is the regularization term, based on the l_1 norm. λ is the trade-off parameter controlling the relative strength between the data misfit and the number of nonzero coefficients $\mathbf{a}$, see Chen et al. (2001) [7], Vera Rodriguez et al. (2012) [17].

Basis pursuit converges to a local optimum. The performance of this method is strongly dependent on the predefined wavelet dictionary. Combining different dictionaries to make bigger, more complete dictionaries can enhance basis pursuit decompositions, see Chen et al. (2001) [7], Rubinstein et al. (2010) [13], but comes at the expense of making matrix D bigger and thus prolonging computation time.

2.5 Complex trace analysis

Complex trace analysis treats a seismic trace, $s(t)$, as the real part of a complex trace, $c(t)$. The complex trace is defined by the following

$$c(t) = s(t) + iH_s(t) \tag{13}$$

where, $H_s(t)$, denotes the Hilbert transform of the signal, $s(t)$. The envelope, $E(t)$, of the signal is defined by

$$E(t) = \sqrt{s^2(t) + H_s^2(t)}. \tag{14}$$

This seismic attribute characterizes the acoustic impedance contrast and therefore is important in reflectivity analysis. Some of the geological features which the envelope is useful in identifying are bright spots, gas accumulation and major lithological changes, see Subrahmanyam (2008) [10].

The first and second time derivatives of the envelope, $E(t)$, are important quantities in complex trace analysis as well.

The first derivative of the envelope is useful, see Subrahmanyam (2008) [10]:

- in identifying sharp interfaces and sharp discontinuities,
- for indicating changes in reflectivity, and
- is related to the absorption of energy.

The second derivative of the envelope is useful, see Subrahmanyam (2008) [10]:

- in identifying sharp changes in lithology,
- in indicating the sharpness of seismic events, and
- shows all reflecting interfaces visible within seismic band-width.

The instantaneous phase attribute is also widely used in seismic data interpretation and is given by

$$\theta(t) = \arctan\left(\frac{H_s(t)}{s(t)}\right). \tag{15}$$

Note that the seismic trace and the Hilbert transform of the trace are related to the envelope and phase by the following:

$$s(t) = E(t)\cos\left[\theta(t)\right], \tag{16}$$

$$H_s(t) = E(t)\sin\left[\theta(t)\right], \tag{17}$$

where $\theta(t) \in (-\pi, \pi)$. The instantaneous frequency is defined by the derivative of $\theta(t)$. The derivative of the instantaneous frequency is the instantaneous acceleration. The instantaneous frequency is useful in the identification of bed thickness and lithological parameters, chaotic reflection zones, and Sand-Shale ratio.

The instantaneous acceleration is employed in the indication of bedding differences between interfaces.

3 Geological data

In this section, we introduce the concepts of seismic acquisition, beginning with a simple ray-based concept and ending with the practical details of the data acquisition procedures in our study. The most simple data collecting procedure would be to use a single source, generating rays normal to the surface of the earth, and a single receiver at some depth beneath the surface. Such an experiment would be called a zero-offset experiment because there is no offset distance between source and receiver. This procedure in practice is never done however due to seismic noise.

One common procedure in data acquisition is called the Common-Mid-Point method, which is usually shortened to CMP. The idea of the method is to acquire a series of traces which represent the source rays at varying offsets reflected at a CMP.

Signals generated from different sources at varying offset positions result in a curved series of arrivals of the seismic traces. This is due to the signals traveling from farther offsets taking longer to reach the CMP than signals traveling from closer offsets. The trace curve is hyperbolic and is related to travel time, offset and velocity of the signals. The trace curve must be corrected such that the seismic events line up on the gather, which is a horizontal line when the corrected traces are lined up vertically in a row. This is called Normal Moveout Correction.

The procedure of summing the corrected traces incident on the CMP is an important technique in data acquisition and is called stacking. Seismic traces before averaging are said to be pre-stack data. When the traces are summed resulting in an increased signal to noise ratio, the data is said to be post-stack data.

An example of pre and post stack data for both valleys and reservoirs are shown in Fig. 1 (pre-stack reservoir data) and 2 (post-stack reservoir and valley data).

4 Post-stack data results

We begin by evaluating the performance of various attributes on the post-stack reservoir data sets described in section 3.

We started by testing standard attributes for identification of hydrocarbon reservoirs or valleys on the post-stack seismic data. It is worth noting that these attributes do not require any time-frequency analysis, and can be calculated directly from the trace data. Fig. 3 shows the first and second derivatives of the envelope for the reservoir data set. We note that these standard attributes are able to capture the location of the reservoir, but are known to under-perform for more complicated data sets. For instance, Fig. 4 shows the same attributes for the seismic data associated with a valley. The first derivative of the envelope does not seem to reveal any useful information about the location of the valley. The second derivative of the envelope fares slightly better but does not provide an accurate localization. Other standard attributes such as instantaneous frequency or instantaneous bandwidth failed to identify the relevant structures (reservoir and valley) in both seismic data sets (results not shown).

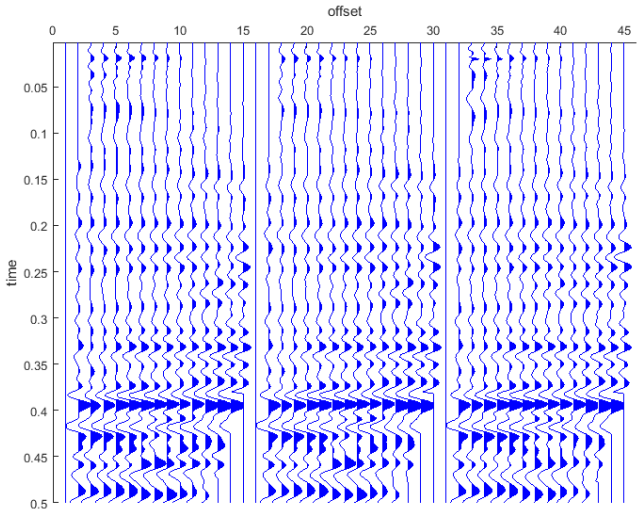

Fig. 1 Pre-stack data corresponding to the reservoir data in Fig. 2.

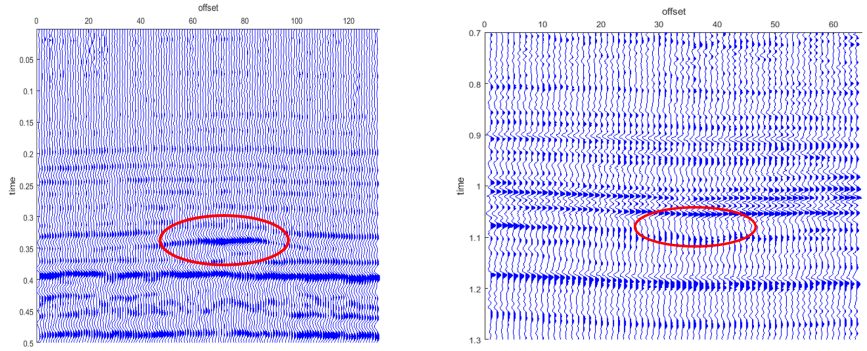

Fig. 2 Post-stack data where the goal is to identify a hydrocarbon reservoir around offsets $60-85$ and time $0.34s$ (left) and a valley at offsets $30-40$ and time $1.05s$ (right)

Now, we consider the various spectral decomposition methods we used to test amplitude and phase attributes. Recall these methods include Short-Time Fourier Transform (STFT), Continuous Waveform Transform (CWT), Synchrosqueezing Transform (SST) and Basis Pursuit (BP).

Amplitude and phase attributes given by the STFT spectral decomposition method are first investigated for the available seismic data sets. Unfortunately, this method does not provide high resolution images for the reservoir post-stack data set (see Fig. 5). We also test this method on the valley post-stack data set. We can actually

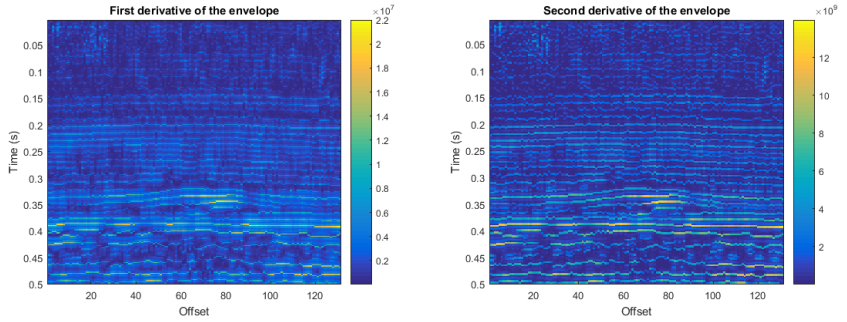

Fig. 3 Attributes for the reservoir post-stack data: First derivative of the envelope (left) and second derivative of the envelope (right)

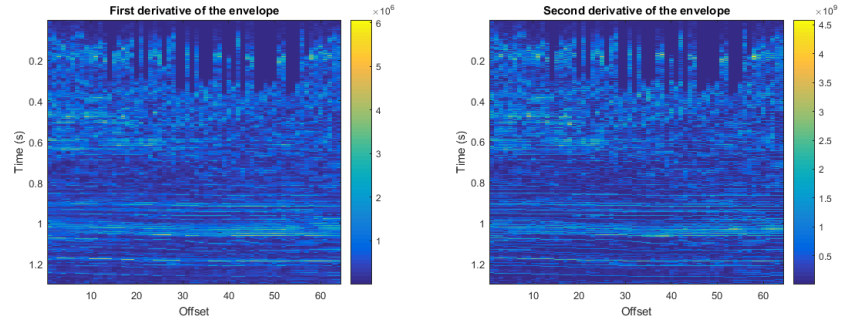

Fig. 4 Attributes for the valley post-stack data: First derivative of the envelope (left) and second derivative of the envelope (right)

spot a valley in time zone from 1s to 1.1s in the figures. Some promising results are shown in Fig. 6.

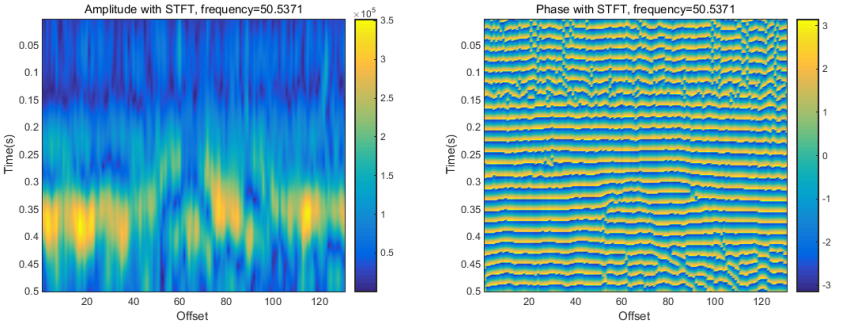

Fig. 5 Amplitude (right) and phase (left) for the reservoir post-stack data: Constant frequency slice obtained with STFT at approx. 50.5 Hz.

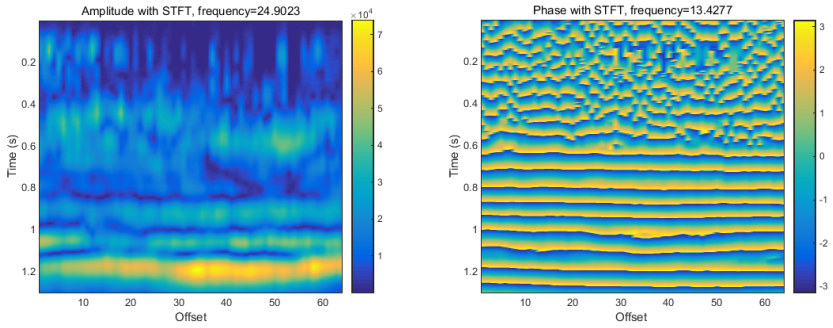

Fig. 6 Amplitude (right) and phase (left) for the valley post-stack data: Constant frequency slices obtained with STFT at approx. 24.9 Hz and 13.4 Hz, respectively.

We continue by discussing the results from CWT. Recall from section 2 that the CWT method depends upon a mother wavelet. We tested a Morlet, a Ricker and a Gauss wavelet dictionary and concluded that the CWT produced better results using the Morlet family of wavelets. The resolution for CWT results is not clear with regards to the amplitude; despite this, we can recognize the presence of a reservoir in Fig. 7 (left). CWT provides a much clearer resolution for the phase attribute as we can see from Fig. 7 (right).

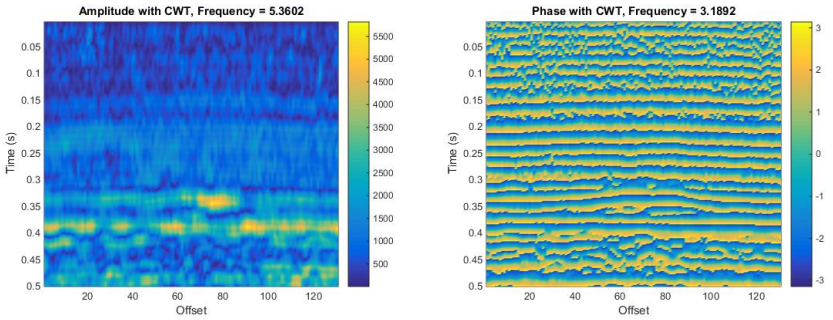

Fig. 7 Amplitude (right) and phase (left) for the reservoir post-stack data: Constant frequency slices obtained with CWT at approx. 5 Hz and 3 Hz respectively. CWT was performed with a Morlet wavelet dictionary.

With respect to the valley data, CWT performs more adequately for the amplitude attribute than phase attribute (Fig. 8). The method provides a high resolution plot for the amplitude attribute where we can recognize the presence of a valley, while for the phase attribute, the localization of the valley is not as clear.

We also applied the SST spectral decomposition method to the data sets. We began by considering the reservoir data. Note that this method also requires a mother wavelet. Similar to the CWT method, we found that the Morlet wavelet provides

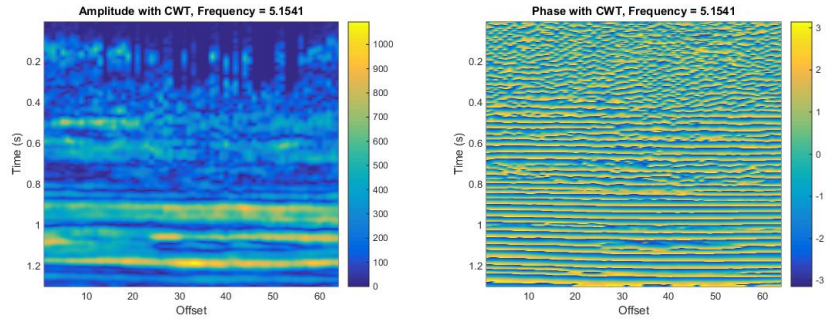

Fig. 8 Amplitude (right) and phase (left) for the valley post-stack data: Constant frequency slices obtained from CWT at approx. 5 Hz (both). CWT was performed with a Morlet wavelet dictionary.

better results than the Ricker and the Gauss wavelet family. As such, we used this wavelet to obtain the following results for SST. Observe that the amplitude attribute has low resolution; however, we can still locate the reservoir, see Fig. 9 (left). Despite the low resolution, the phase attribute has a higher resolution than the amplitude attribute, and we can detect the presence of the reservoir, see Fig. 9 (right).

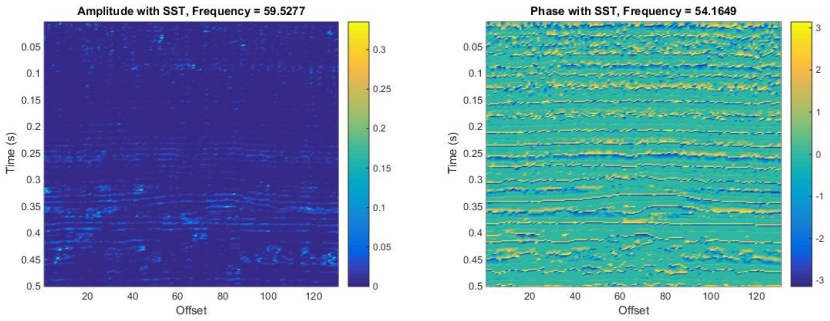

Fig. 9 Amplitude (right) and phase (left) for the reservoir post-stack data: Constant frequency slices obtained with SST at approx. 60 Hz (left) and 55 Hz (right). SST was performed with a Morlet wavelet dictionary.

SST performs less adequately for the valley data. The resolution for both the amplitude and phase attributes is low; however, while we can still locate the valley in both images from Fig. 10, it is considerably more difficult than other spectral decomposition methods.

We also test the amplitude and phase attributes given by the BP spectral decomposition method for the available seismic data sets. This method provides high resolution images as can be seen in Fig. 11. We note that the localization of the reservoir is clear in all frequency slices in the amplitude plots (left). The phase attribute for reflected waves at constant frequency are used less often, but the right

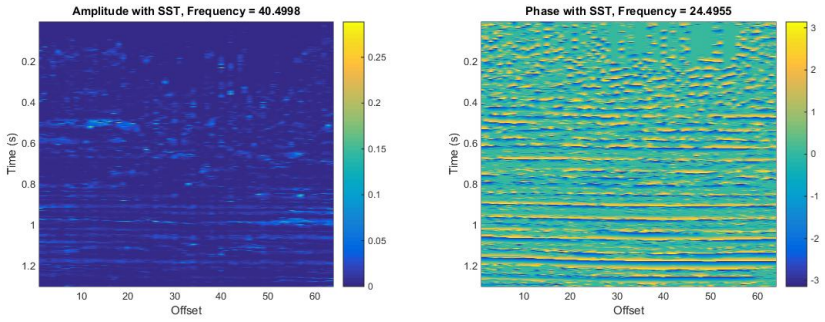

Fig. 10 Amplitude (right) and phase (left) for the valley post-stack data: Constant frequency slices obtained with SST at approx. 40 Hz (left) and 25 Hz (right). SST was performed with a Morlet wavelet dictionary.

plots of Fig. 11 show promise in the use of this attribute for reservoir identification. The darker blue curved areas show the consistency of this attribute throughout a range of frequencies.

The phase attribute was also tested on the post-stack data where identification of a valley is of relevance (see right plot of Fig. 2). Fig. 12 shows that the phase attribute calculated using the BP spectral decomposition method can accurately identify the valley in the $20-35$ Hz frequency range. Just as in the reservoir case, BP proves to be the method that led to the most consistent and high resolution localization results.

To visualize these phase attribute plots even better and remove the coherent horizontal lines from figures such as Fig. 12, we propose a correction method. This consists of unwrapping the time-dependent curve in the phase attribute for each frequency and offset, and fitting this curve to a quadratic equation. We then subtracted the resulting quadratic curve from the unwrapped time-dependent phase. The reasoning for such an approach is that the residual obtained after this subtraction may remove the artificial straight lines from the phase attribute curves while maintaining localization information about the valley.

Our analysis shows that the derivative of the residual phase attribute obtained from this correction method shows promise in identifying certain structures such as the valley in this data set. Fig. 13 shows frequency slices of the derivative of the residual. We note that the valley seems to be localized inside the darker lines at approximately 1.1s. We expect this method to uncover the boundaries of the structure given that the derivative of the residual phase curve can point to significant changes in phase. We also note that Fig. 13 could potentially be more useful than Fig. 12 since it may highlight actual geological structure changes that are not clear in the phase attribute plots.

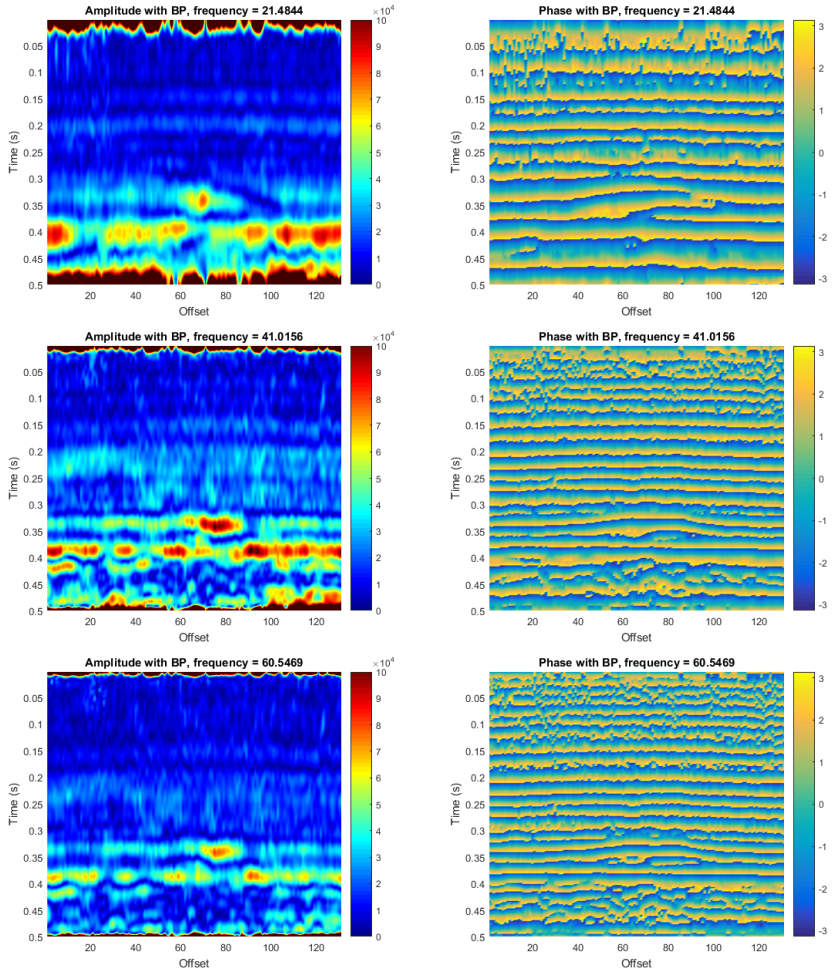

Fig. 11 Amplitude (right) and phase (left) for the reservoir post-stack data: Constant frequency slices obtained with BP at approx. 20 Hz (top), 40 Hz (center) and 60 Hz (bottom). BP was performed with a Ricker wavelet dictionary. The Matlab *jet* scale was used for the amplitude figures in the left plots for better visualization.

5 Pre-stack data analysis – AVO

5.1 AVO background

Unlike density, seismic velocity involves the deformation of a rock as a function of time. A cube of rock can be compressed, which changes its volume and shape; or sheared, which changes its shape but not its volume. This leads to two different types of velocities: P-wave, or compressional wave velocity, in which the particle

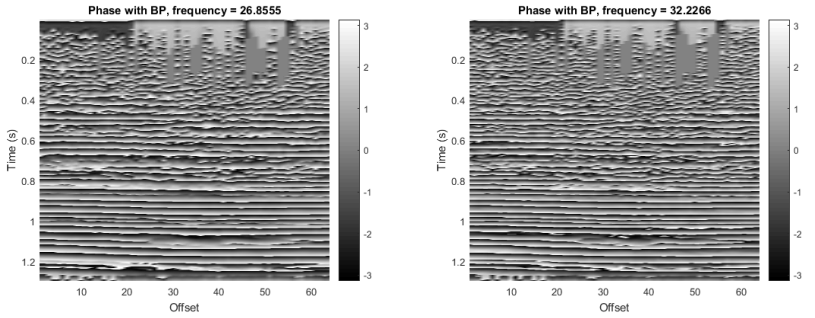

Fig. 12 Phase for the valley post-stack data: Constant frequency slices obtained with BP at approx 27 Hz (left), and 32 Hz (right). BP was performed with a Ricker wavelet dictionary. The Matlab *gray* scale was used for better better visualization.

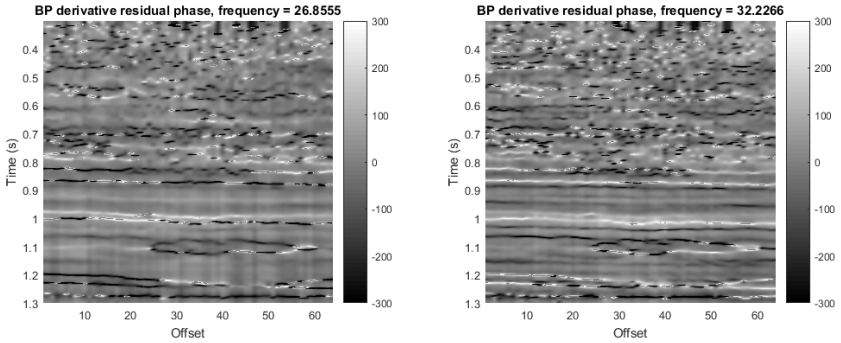

Fig. 13 Derivative of the residual phase for the valley post-stack data: Constant frequency slices obtained with BP for the derivative of the residual phase attribute at approx 27 Hz (left), and 32 Hz (right). BP was performed with a Ricker wavelet dictionary. The Matlab *gray* scale was used for better better visualization.

moves is in the same direction as the wave; S-wave, or shear wave velocity, in which the particle moves perpendicular to the wave movement. If the incident angle is not perpendicular to the reflecting surface, an incident P-wave will produce both P and S reflected and transmitted waves. This is called mode conversion, see Fig. 14 for an illustration. We utilize mode conversion to analyze pre-stack data in two ways: (1) Record the converted S-waves using three-component receivers (in the X, Y and Z directions); (2) Interpret the amplitudes of the P-waves as a function of offset, or angle, which contain implied information about the S-waves. We use approach (2), which is called the Amplitude versus Offset (AVO) method.

In the AVO method, we can employ the Zoeppritz equations, or an approximation of these equations, to extract S-wave type information from P-wave reflections at different offsets. We would like to note that though seismic data is recorded as a function of offset, there is a direct relationship between angle and offset, which depends on velocity, and we can convert the seismic data from offset domain to angle

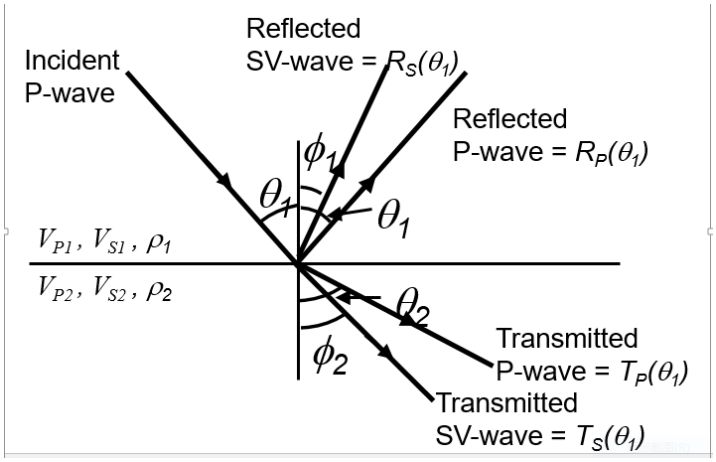

Fig. 14 Illustration of Mode Conversion of an Incident P-Wave.

domain, see an example in Fig. 15. We will model the amplitude changes on angle converted data sets.

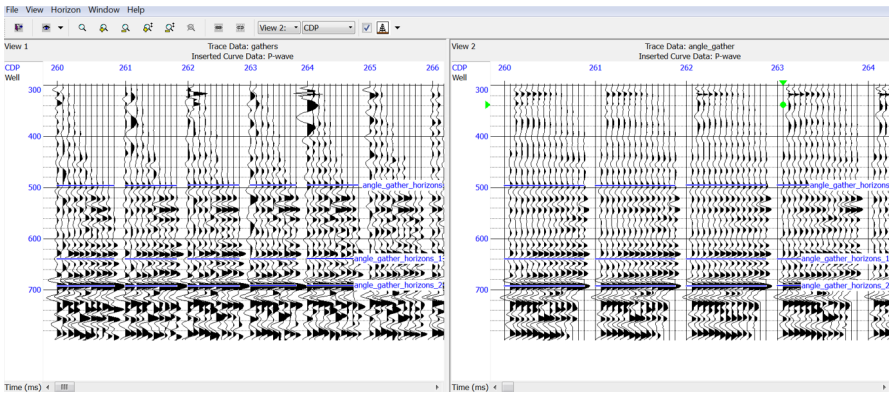

Fig. 15 Seismic data converted from offset domain to angle domain.

5.2 Conventional AVO

Zoeppritz derived the amplitudes of the reflected and transmitted waves using the conservation of stress and displacement across the layer boundary. Although the Zoeppritz equations give us the exact amplitudes as a function of angle, they do not

provide an intuitive understanding of the AVO process for positive angles. For this reason, AVO theory for analyzing real data is based on a linearized approximation to the Zoeppritz equations initially derived by Bortfeld (1961) [4] and then refined by Richards et al. (1976) [12] and Aki and Richards (1980) [1]. In this section, we introduce the following Wiggins' form of the Aki-Richards equation [18], which is one of the most commonly used linear AVO approximations. We used this equation in order to perform AVO analysis on pre-stack seismic data:

$$R_P(\theta) = A + B\sin^2\theta + C\tan^2\theta\sin^2\theta, \tag{18}$$

where $A = \frac{1}{2}(\frac{\triangle V_P}{V_P} + \frac{\triangle \rho}{\rho})$ is called the intercept, $B = \frac{1}{2}\frac{\triangle V_P}{V_P} - 4(\frac{V_S}{V_P})^2\frac{\triangle V_S}{V_S} - 2(\frac{V_S}{V_P})^2\frac{\triangle \rho}{\rho}$ is called the gradient, $C = \frac{1}{2}\frac{\triangle V_P}{V_P}$ is called the curvature [5, 6]. We note that the last term of Eqn. (18) is often ignored. In Fig. 16, we show fitting results of Eqn. (18) using the pre-stack reservoir data. The attributes A and B are plotted at each offset and time sample.

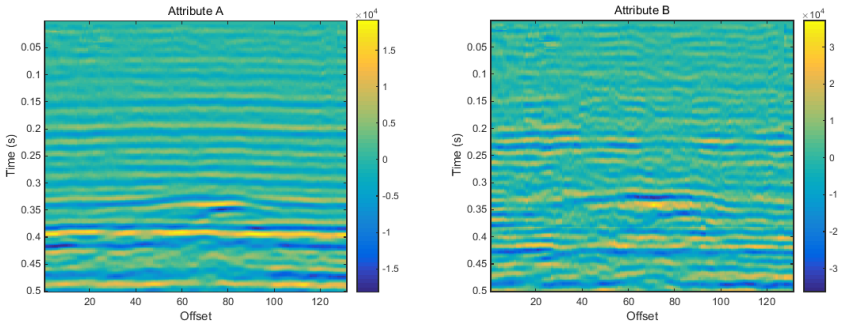

Fig. 16 Attributes A (left) and B (right) as a function of time and offset.

5.3 Wiggins frequency AVO

Attributes A and B calculated in the previous subsection are often useful in analyzing pre-stack data, and have a clear physical interpretation given their connection to rock density as well as P-wave and S-wave velocities. While these attributes highlight the reservoir area very well in our example (see Fig. 16), they often fail for more complicated and noisy seismic data. Our goal in this subsection is to determine whether spectral decomposition methods can provide additional attributes that are helpful in identifying hydrocarbon reservoirs.

Both the Wiggins form of the Aki-Richards equations used above and the Zoeppritz equations from which they are derived, assume that the frequency of the re-

flected wave solutions is constant. This turns out not to be the case in actual seismic experiments. As a result, an equation that incorporates frequency information would be useful in deriving more accurate data attributes.

One approach would be to extend the spectral decomposition method to signals at a certain angle θ associated with a CMP and then use the approximation for the amplitude of the reflected waves given by Eqn. (18). We illustrate this approach with STFT. We fix location x and then consider the seismic trace, $s_\theta(t)$, associated with fixed angle θ. Applying the STFT transform, we obtain:

$$S_s(f,\tau) = \int_{-\infty}^{\infty} s_\theta(t) w(t-\tau) e^{-2i\pi ft} dt\,. \tag{19}$$

Assuming that the approximation given by the Wiggins form of the Aki-Richards equation holds, we have that

$$s_\theta(t) = A(t) + B(t)\sin^2\theta\,. \tag{20}$$

Plugging equation (20) into (19) yields

$$S_s(f,\tau) = T_1(\tau,f) + T_2(\tau,f)\sin^2\theta\,, \tag{21}$$

where $T_1(\tau,f) = \int_{-\infty}^{\infty} A(t) w(t-\tau) e^{-2i\pi ft} dt$ and $T_2(\tau,f) = \int_{-\infty}^{\infty} B(t) w(t-\tau) e^{-2i\pi ft} dt$. T_1 and T_2 are thus attributes that vary not only with offset and time, but also with frequency. Similar to the analysis of attributes A and B, we aim to understand the performance of T_1 and T_2 in revealing hydrocarbon reservoirs.

This approach can be generalized to all the spectral decomposition methods in section 2, since the only difference lies in the family of wavelets used. Given the success of BP in identifying both the reservoir and valley in our examples for post-stack data sets, we used this method in order to derive the T_1 and T_2 functions above for the pre-stack reservoir data in Fig. 1. Fig. 17 shows the result of the BP spectral decomposition and fitting to equation (21). The attributes are plotted at a frequency of about 37 Hz, where the reservoir location seems best highlighted. The results localize the hydrocarbon reservoir but are not more convincing than the standard A, B attributes obtained directly from signal data (see Fig. 16).

We found that a more convincing attribute for this pre-stack reservoir data set is $T_1(f) \times T_2(f)$, of which we show frequency slice plots in Fig. 18. This attribute (corresponding to the product of intercept and gradient) is known to have a physical interpretation and localizes the reservoir through a large range of frequencies (40 - 80 Hz). The attribute varies with frequency and fades at very low and very high frequency values.

We further investigated the Wiggins frequency AVO method given by equation (21) in order to determine if this technique can distinguish between different types of reservoirs. In particular, we considered two sets of synthetic data as shown in Fig. 19. The left panel corresponds to a brine reservoir while the right panel shows the location of a gas reservoir. In both cases, the top of the reservoir is at about 627 ms and the bottom at about 636 ms. The brine reservoir case is often called an anomaly

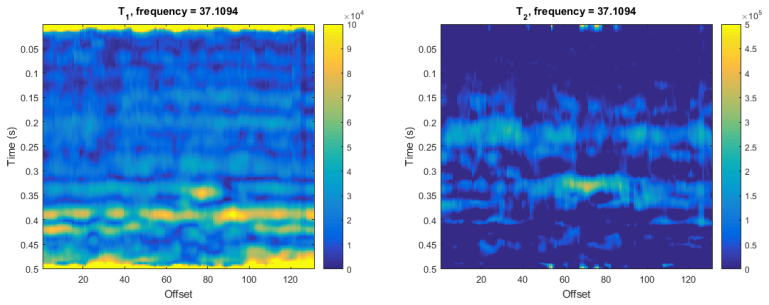

Fig. 17 Attributes T_1 (left) and T_2 (right) at approx 37 Hz as a function of time and offset. BP was performed with a Ricker wavelet dictionary.

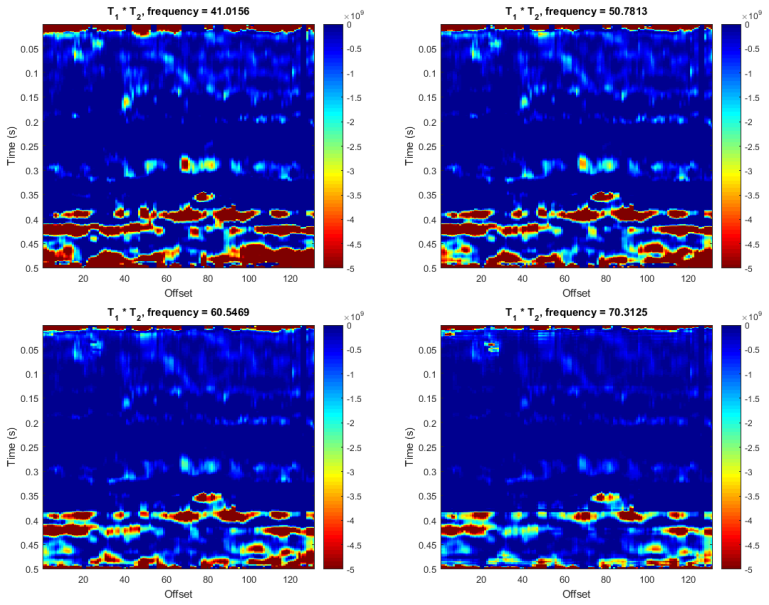

Fig. 18 Attribute $T_1 \times T_2$ at approx 40, 50, 60 and 70 Hz. BP was performed with a Ricker wavelet dictionary.

of Class 1 when analyzing the A and B attributes in equation (18). On the other hand, the gas reservoir which is typically of interest is a Class 3 anomaly.

Fig. 19 shows the difference between these two classes of reservoirs. The top of the gas reservoir consists of well-defined waves of similar amplitude and phase that are consistent across different angle sources, while the top of the brine reservoir is considerably less regular. The results of the Wiggins frequency AVO method on these data sets are shown in Fig. 20 and 21. We note that the $T_1(f)$ attribute identifies the reservoirs around frequencies $15-25$ Hz while the $T_2(f)$ attribute identifies the reservoirs at frequencies $12-20$ Hz. Attribute $T_1(f)$ (left panel of Fig. 20 and 21)

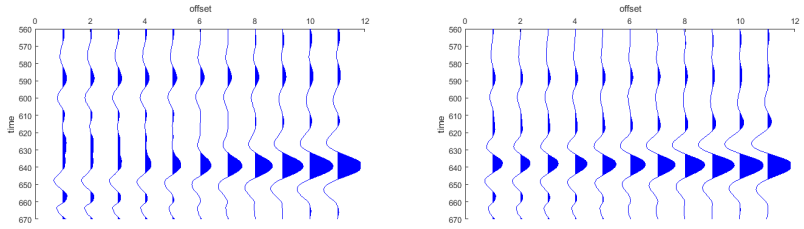

Fig. 19 Portions of synthetic data sets for a brine reservoir (left) and a gas reservoir (right) for a single offset with 11 angle sources.

seems to perform best at distinguishing between the reservoirs as it shows a much brighter spot for the gas data set. Attribute $T_2(f)$ (right panel of Fig. 20 and 21) seems less proficient at identifying the different-class reservoirs, even though its values are slightly lower for the brine data set.

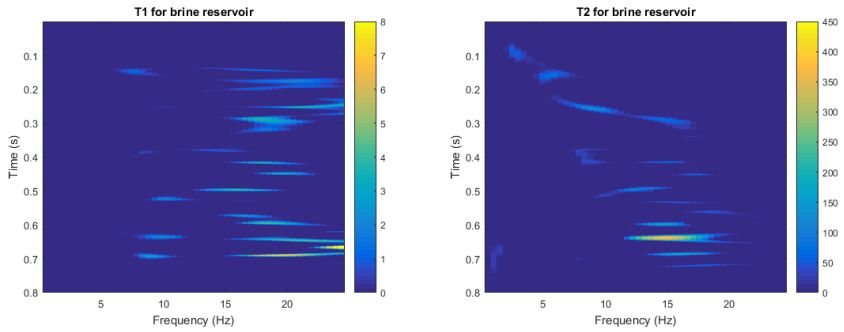

Fig. 20 Attributes T_1 (left) and T_2 (right) for the brine reservoir as a function of time and frequency. BP was performed with a Ricker wavelet dictionary.

5.4 Smith-Gidlow frequency AVO

In the method introduced by Stolt and Weglein (1985) [16], elastic parameters can be estimated through seismic reflection information. Smith and Gidlow (1987) [15] described how to apply time and offset-variant weights to seismic data in order to extract P-wave and S-wave fractional velocities which are defined as $\Delta V_P/V_P$ and $\Delta V_S/V_S$, respectively. The two-term Smith-Gidlow AVO approximation assumes the following form:

$$R(\theta) = P(\theta)\frac{\Delta V_P}{V_P} + Q(\theta)\frac{\Delta V_S}{V_S}, \tag{22}$$

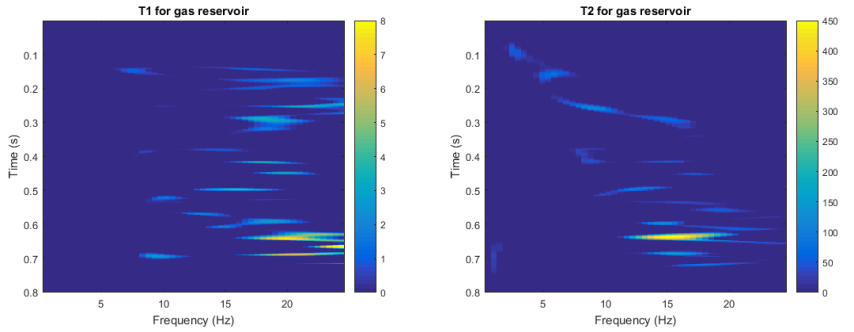

Fig. 21 Attributes T_1 (left) and T_2 (right) for the gas reservoir as a function of time and frequency. BP was performed with a Ricker wavelet dictionary.

where $P(\theta) = \frac{5}{8} - \frac{V_S^2}{2V_P^2} sin^2\theta + \frac{1}{2} tan^2\theta$, $Q(\theta) = -4\frac{V_S^2}{V_P^2} sin^2\theta$. We combine Wilson (2010) [19, 21] with the idea for Wiggins frequency AVO method explored in section 5.3 and make the assumption that the constants $P(\theta)$ and $Q(\theta)$ are frequency-independent and do not vary with velocity dispersion. Applying spectral decomposition methods to our pre-stack seismic data, we can extend the elastic Smith-Gidlow AVO approximation (22) to a frequency-dependent equation,

$$R(\theta, f) = P(\theta)\frac{\Delta V_P}{V_P}(f) + Q(\theta)\frac{\Delta V_S}{V_S}(f), \tag{23}$$

which we call Smith-Gidlow frequency AVO approximation. We note that the fractional velocities $\Delta V_P/V_P$and $\Delta V_S/V_S$ are attributes that vary not only with offset and time, but also with frequency. Moreover, we introduce two terms related to P-wave and S-wave reflectivity dispersion as in Wilson (2010) [19, 21], I_a and I_b Thee attributes are defined as the derivatives of $\frac{\Delta V_P}{V_P}$ and $\frac{\Delta V_S}{V_S}$ with respect to frequency, respectively. The forward scheme of finite differences is used in the evaluation of $\frac{\Delta V_P}{V_P}$ and $\frac{\Delta V_S}{V_S}$, which gives

$$I_a(f_i) = \frac{\Delta V_P/V_P(f_{i+1}) - \Delta V_P/V_P(f_i)}{f_{i+1} - f_i}, \tag{24}$$

$$I_b(f_i) = \frac{\Delta V_S/V_S(f_{i+1}) - \Delta V_S/V_S(f_i)}{f_{i+1} - f_i}, \tag{25}$$

where $\{f_i\}$ are the discrete frequency steps.

We aim to understand the performance of $\Delta V_P/V_P$, $\Delta V_S/V_S$, I_a and I_b in revealing hydrocarbon reservoirs. In this section, we use BP as our spectral decomposition technique to derive the spectral amplitudes at a series of frequencies. When $R(\theta, f)$ is replaced by the spectral amplitude at different frequencies, we can make use of least-squares method to estimate $\Delta V_P/V_P$, $\Delta V_S/V_S$, I_a and I_b. Considering that the shear modulus is usually independent of the saturating fluid, we focus on

the $\Delta V_P/V_P$ and I_a attributes to estimate the magnitude of P-wave dispersion which are our new FAVO attributes. Fig. 22 shows the frequency slice results of the BP spectral decomposition and fitting $\Delta V_P/V_P$ and I_a by using the pre-stack reservoir data set. The results are convincing since we can identify the location of the hydrocarbon reservoir.

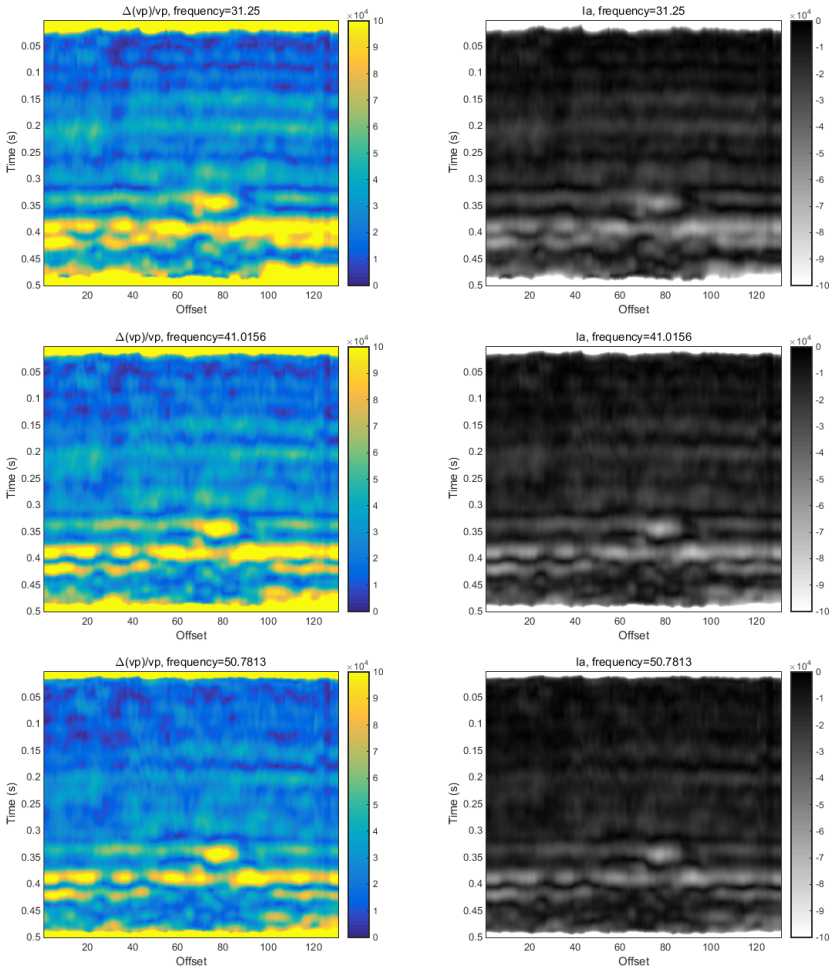

Fig. 22 Attributes $\Delta V_P/V_P$ (left) and I_a (right) for the reservoir pre-stack data: Constant frequency slices at approx. 30 Hz (top), 40 Hz (center) and 50 Hz (bottom) as a function of time and offset. BP was performed with a Ricker wavelet dictionary.

We note that one of the main novelties of the approach in this section is that we use BP for spectral decomposition while Wilson (2010) [19, 21] makes use of the Wigner-Ville distribution, which is a conventional time-frequency method. This

means that we obtain better resolution for the frequency slices and can better identify hydrocarbon reservoir locations. Moreover, we use the finite difference scheme in calculating I_a and I_b in equations (24) and (25). Wilson (2010) [19, 21] employs a Taylor expansion of $R(\theta, f)$ in equation (23) at a central frequency and the least-squares method to determine these fractional velocity derivatives. The finite difference scheme simplifies the approach and makes our proposed Smith-Gidlow FAVO method an efficient and easy to implement technique for determining frequency-dependent information for pre-stack data.

6 Conclusions

In this paper, we explored several seismic data analysis methods that were used to identify hydrocarbon reservoirs in the subsurface of the earth. Standard attributes such as derivatives of the envelope and the instantaneous frequency provided a benchmark to compare with the attributes obtained by time-frequency decomposition methods. The methods examined in this paper included $STFT$, CWT, SST and BP. We found the method of BP with Ricker wavelets gave the best results for a wide range of frequencies in the examination of our post-stack data sets.

AVO methods, which are pre-stack data analysis tools, were also considered in this paper. We first applied the conventional AVO method on Wiggins' form of the Aki-Richards equation to pre-stack data and determined the location of the reservoir. AVO integrated with spectral decomposition allowed us to develop two frequency AVO (FAVO) methods. Compared with conventional AVO, FAVO methods using BP time-frequency analysis exhibited better resolution as well as encoded frequency-dependent information. These methods show promise in identifying hydrocarbon reservoirs and other geological structures, and can be investigated further on other data sets.

Acknowledgements

This work is the product of the IMA/PIMS Graduate Student Mathematics Modeling in Industry Workshop of 2015, sponsored by the Institute for Mathematics and its Applications and the Pacific Institute for the Mathematical Sciences. We thank these institutions for organizing and hosting the event, and funding the participation of the authors of this report. CGG and the CREWES consortium of Calgary, Alberta graciously provided both data and software tools for the project. We would also like to thank our mentors, Dr. Jiajun Han of CGG, and Dr. Michael Lamoureux of the University of Calgary for their continued guidance.

References

1. Aid, K., Richards, P.: Quantitative seismology: Theory and methods. San Francisco (1980)
2. Auger, F., Flandrin, P.: Improving the readability of time-frequency and time-scale representations by the reassignment method. IEEE Tansactions on Signal Processing **43**, 1068–1089
3. Bonar D, ., M.Sacchi: Complex spectral decomposition via inversion strategies. SEG Annu. Meeting Abstr. pp. 1408–1412 (2010)
4. Bortfeld, R.: Approximations to the reflection and transmission coefficients of plane longitudinal and transverse waves*. Geophysical Prospecting **9**(4), 485–502 (1961)
5. Castagna, J.P., Swan, H.W.: Principles of avo crossplotting. The leading edge **16**(4), 337–344 (1997)
6. Castagna, J.P., Swan, H.W., Foster, D.J.: Framework for avo gradient and intercept interpretation. Geophysics **63**(3), 948–956 (1998)
7. Chen S. S., D.L.D., Saunders, M.: Atomic decomposition by basis pursuit. SIAM Rev **43(1)**, 129–159
8. Cohen, L.: Time-frequency analysis: Theory and applications. Prentice Hall, Englewood Cliffs, NJ (1995)
9. Daubechies, I.: Ten lectures on wavelets. SIAM, CBMS-NSF Regional Conference Series in Applied Mathematics (1992)
10. D.Subrahmanyam, P.: Seismic attributes- a review. 7th International Conference and Exposition on Petroleum Geophysics pp. 398–405 (2008)
11. Li, C., Liang, M.: A generalized synchrosqueezing transform for enhancing signal time-frequency representation. Signal procesing **92**, 2264–2274 (2012)
12. Richards, P.G., Frasier, C.W.: Scattering of elastic waves from depth-dependent inhomogeneities. Geophysics **41**(3), 441–458 (1976)
13. Rubinstein R., A.M.B., M., E.: Dictionaries for sparse representation modeling. Proc. IEEE **98(6)**, 1045–1057
14. Sinha, S.: Time-frequency localization with wavelet transform and its application in seismic data analysis. Society of Industrial and Applied Mathematics **M.S. thesis, University of Oklahoma**
15. Smith, G., Gidlow, P.: Weighted stacking for rock property estimation and detection of gas. Geophysical Prospecting **35**(9), 993–1014 (1987)
16. Stolt, R., Weglein, A.: Migration and inversion of seismic data. Geophysics **50**(12), 2458–2472 (1985)
17. Vera Rodriguez I., D.B., Sacchi, M.D.: Microseismic data denoising using a 3c group sparsity constrained time-frequency transform. Geophysics **77**, V21–V29
18. Wiggins, R., Kenny, G., McClure, C.: A method for determining and displaying the shear-velocity reflectivities of a geologic formation: European patent application 0113944 (1983)
19. Wilson, A.: Theory and methods of frequency-dependent avo inversion (2010)
20. Wu H.-T., P.F., Daubechies, I.: One or two frequencies? the synchrosqueezing answers. Advances in Adaptive Data Analysis **3(2)**, 29–39 (2011)
21. Wu, X., Chapman, M., Li, X.Y.: Frequency-dependent avo attribute: theory and example. First Break **30**(6), 67–72 (2012)
22. Zhang, R., J., C.: Seismic sparse-layer reflectivity inversion using basis pursuit decomposition. Geophysics **76(6)**, R147–R158